CI emission from the outflow and PDR in S140

Astron. Astrophys. 291, 250–260 (1994)

ASTRONOMY AND ASTROPHYSICS

C I emission from the outflow and PDR in S 140

Nigel R. Minchin [1], **Glenn J. White** [1], **Juergen Stutzki**[2], **and Dirk Krause**[2]

[1] Department of Physics, Queen Mary and Westfield College, University of London, Mile End Road, London E1 3NS, UK
[2] Physikalisches Institut, Universität zu Köln, Zülpicher Straße 77, D-50937 Köln, Germany

Received 25 February 1994 / Accepted 4 May 1994

Abstract. We present high resolution maps (10-14 arcsec FWHM) of the atomic carbon [CI]] $^3P_1 \rightarrow ^3P_0$ (492.1607 GHz) fine structure line and the $C^{17}O$ J = 3→2 (337.0611 GHz) rotational line from the outflow and photon-dominated region (PDR) in S 140. These observations reveal remarkable, previously unresolved structure.

There is a marked variation in CI line profiles across the mapped region. Towards the outflow the lines are broad (FWHM ~5-6 km s^{-1}) with peak values of T_{mb} ~10-12K, yet towards the PDR the lines are distinctly narrower (~3-4 km s^{-1}) with higher values of peak T_{mb}, up to 18K.

Both the CI and $C^{17}O$ integrated intensity maps show a similar morphology. The emission peak lies towards the molecular outflow source, and there is an arc of emission extending from the peak towards the south. The CI and $C^{17}O$ arcs are offset, with the CI arc offset to the northeast. This CI arc feature is observed at blue and redshifted velocities, whilst the $C^{17}O$ arc feature is only observed in blueshifted emission. This implies the CI emission lies on the inner edge of the blueshifted molecular outflow wall (traced by the $C^{17}O$ emission). Towards the molecular outflow source the abundance ratio $N(CI)/N(CO)$ = 0.14, with a similar ratio found for the blue wing and core velocity intervals (0.12). The red wing has a particularly high abundance, $N(CI)/N(CO)$ = 0.67. The most plausible mechanism for producing the CI emission is the effect of shocks on the chemical and physical processes at the interface between the stellar wind and the blueshifted outflow cavity wall.

The PDR is a clumpy, narrow (~0.1–0.15pc) elongated ridge-like feature, adjacent to the south-western edge of the molecular cloud. Emission from the PDR is observed across a relatively narrow velocity range, -10 to -6 km s^{-1}. There is a localised integrated emission peak (at offset position -28, -42 arcsec), which we have designated PDRc1 (PDR clump 1). The abundance of CI is particularly high, $N(CI)/N(CO)$ = 0.29 at the position of PDRc1. The observed column density ($9.7\pm0.8\times10^{17}$ cm^{-2}) and emergent intensity ($8.7\pm0.7\times10^{-6}$ erg cm^{-2} s^{-1} sr^{-1}) towards PDRc1 are in close agreement with recent modelling of low-density PDRs.

Key words: stars: early-type – interstellar medium: HII regions – jets and outflows

1. Introduction

The origin and relative abundance of atomic carbon (CI) is of fundamental importance to developing a full understanding of the chemical and physical processes within molecular clouds. Several large-scale studies have been published (e.g. Phillips & Huggins 1981; Wootten et al. 1982; Keene et al. 1985) at low angular resolution (of-the-order 1 arcmin). These observations imply the CI/CO abundance is high, even in the dense cores of clouds (≥0.1). This contradicts gas-phase chemistry models which predict CI should only be abundant near cloud surfaces, due to the photodissociation of CO by interstellar UV radiation. In the deep interiors virtually all carbon should be locked in CO (e.g. Langer 1976; Prasad & Huntress 1980). There are several different models that have attempted to explain the production of CI deep within molecular clouds. These include the effects of UV radiation from embedded young stars, cosmic rays and shocks produced in high-velocity molecular outflows (e.g. Hollenbach & McKee 1989). Another possibility is that the neutral component of high-velocity stellar winds may be a source of atomic carbon (e.g. Glassgold et al. 1991). It has been suggested that additional sources of atomic carbon are unnecessary if molecular clouds are sufficiently "clumpy" (e.g. Stutzki et al. 1988). This would allow UV radiation to penetrate to far higher depths than would be possible if molecular clouds were composed of uniform-density material.

To increase our understanding of the origin and abundance of CI relative to CO we have mapped the [CI] $^3P_1 \rightarrow ^3P_0$ (492.1607 GHz) and $C^{17}O$ J = 3→2 (337.0611 GHz) line emission from L1204/S 140 at high angular resolution (10 and 14 arcsec FWHM beamsize respectively). The advantage of mapping $C^{17}O$ emission is that, unlike ^{12}CO, ^{13}CO and $C^{18}O$, the line stays optically thin even in the densest core regions. It should therefore be the most accurate high-resolution tracer of the CO morphology.

The L1204 molecular cloud lies to the northeast of the S 140 HII region, produced by the nearby B0 star HD 211880. This molecular cloud is one of the best examples of an edge-illuminated PDR (e.g. Blair et al. 1978; Evans et al. 1987; White & Padman 1991). Only 70-80 arcsec northeast of the PDR is an embedded cluster of three infrared sources (e.g. Beichman et

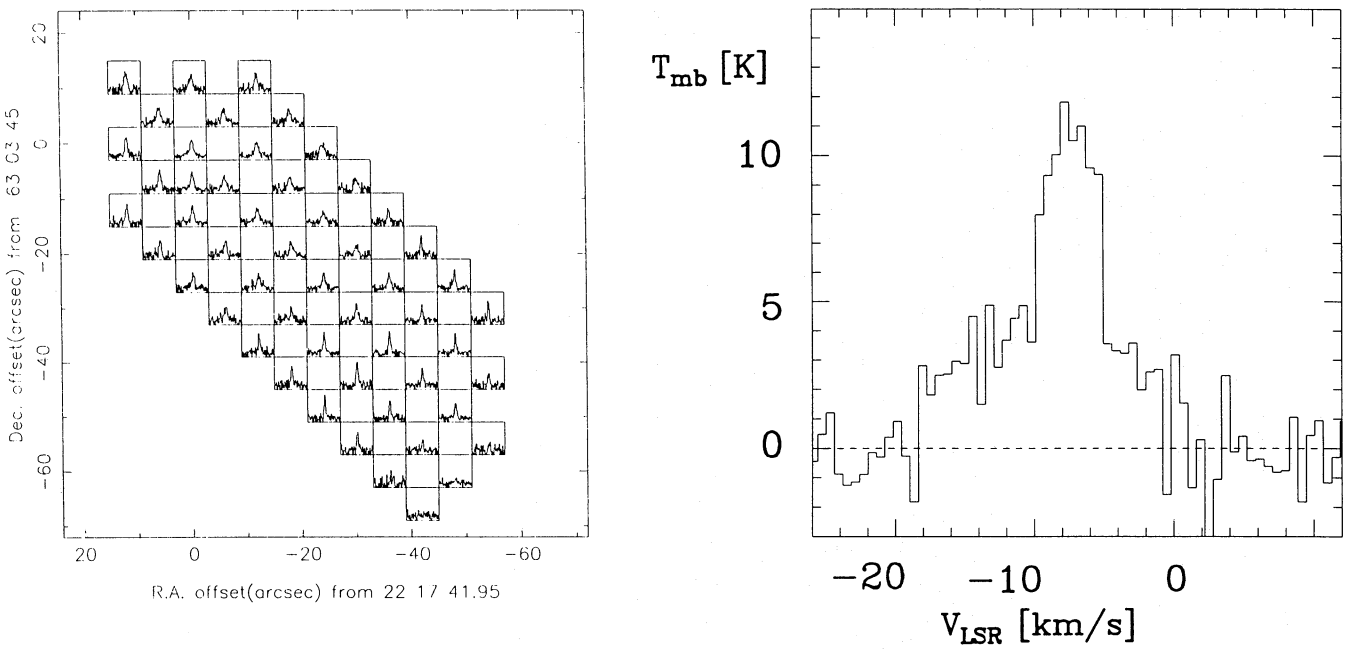

Fig. 1a and b. Observations of the [CI] $^3P_1 \rightarrow {}^3P_0$ line. Shown are **a** a grid of the 51 spectra obtained **b** the line profile observed at the 0,0 position

al. 1979) which lie at the centre of a high-velocity molecular outflow (e.g. Bally & Lada 1983; Snell et al. 1984). The outflow axis is along the southeast-northwest direction, parallel to the PDR. Minchin et al. 1993 (hereafter MWP93) have recently compared single velocity channel [CI] $^3P_1 \rightarrow {}^3P_0$ observations of White & Padman (1991) to various ^{12}CO and ^{13}CO emission line maps. The CI emission is mainly confined to a clumpy, elongated ridge-like feature adjacent to the edge of the molecular cloud and coincident with a similar feature seen in ^{12}CO emission. There is a second region of intense CI emission, located inside a ring of CS emission that surrounds the embedded infrared sources. They conclude that this CI emission may be produced by the outflow or embedded sources.

2. Observations

The observations were obtained in June 1993 using the James Clerk Maxwell Telescope[1] (JCMT), located on Mauna Kea, Hawaii. The receivers used were B3i (310-380 GHz) and C2 (450-504 GHz), both single channel SIS mixer receivers, and were used in conjunction with an acousto-optical spectrometer (see White 1988) with 2048 channels and a total bandwidth of 500 MHz for a single IF channel. The telescope was operated in position switching mode, with an off-source reference 10 arcmin to the south and the east. Tracking and pointing were consistently better than 1 arcsec.

The results presented in this paper have been calibrated in units of corrected main-beam brightness temperature T_{mb} (= T_A^*/η_{mb}) and as such have been corrected for all atmospheric, ohmic, scattering and spillover losses. For the CI and C^{17}O observations we used values of $\eta_{mb} = 0.43$ and 0.53 respectively. The centre position (0,0) for each of the maps is $\alpha_{1950} = 22^h\ 17^m\ 42^s$, $\delta_{1950} = 63^o\ 3'\ 45''$.

[1] The James Clerk Maxwell Telescope is operated by the Royal Observatory, Edinburgh, on behalf of the SERC, the Netherlands Organisation for Pure Research, and the National Research Council of Canada.

3. Results

3.1. The data

Figure 1a presents the CI spectra. There is a marked variation in line profiles across the mapped region. Towards the (0,0) position (the position of peak integrated CO emission) the lines are broad (FWHM ~5-6 km s^{-1}) with peak values of T_{mb} ~10-12K. Further to the southwest (the position of the PDR) the lines are distinctly narrower (~3-4 km s^{-1}) with several positions showing markedly higher values of peak T_{mb}, up to 18K. The (0,0) spectra (Fig. 1b) can be compared directly with the ^{12}CO, ^{13}CO and C^{18}O J = 3→2 and 2→1 spectra observed at the same position using similar beamsizes (14-20 arcsec) shown in Fig. 1 of MWP93. The CI line profile is broad (FWHM ~5 km s^{-1}) with strong and extended blue (between velocities -20 and -10 km s^{-1}) and red (between velocities -5 and 2 km s^{-1}) wings.

These new JCMT observations confirm the detection of broad line wing emission in the [CI] $^3P_1 \rightarrow {}^3P_0$ line by Hernichel et al. (1992), with an integrated intensity comparable to that of the quiescent component. The wing component is T_{mb} ~5K bright at the (0,0) position observed with the high angular resolution of the JCMT. We averaged the JCMT spectra over the region corresponding to the 50 arcsec beam of the KOSMA 3m telescope (Fig. 2). The averaged line shows a wing component with ~2K brightness. The overlay with the spectrum previously observed at KOSMA shows that the calibration between the two telescopes is consistent, as it should be considering that both

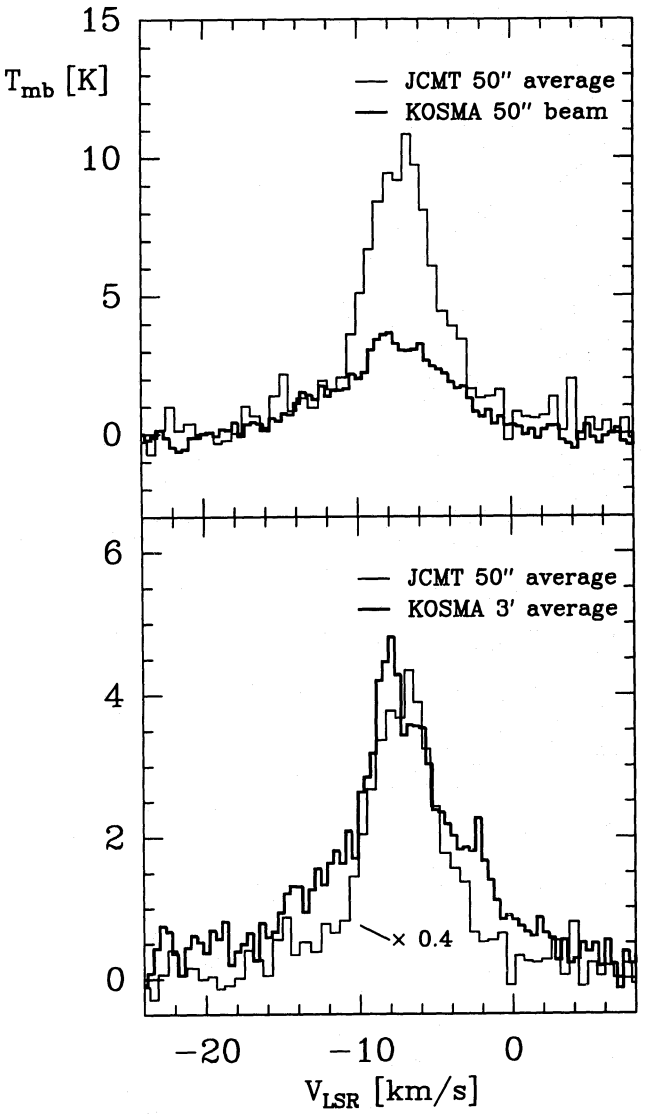

Fig. 2. The averaged JCMT [CI] $^3P_1 \rightarrow {}^3P_0$ spectra observed at the (0,0) position, compared with the spectrum previously observed using the KOSMA 3m telescope (Hernichel et al. 1992)

sets of data were calibrated with a beam efficiency measured on Jupiter with an extent of about 40 arcsec, and that the broad wing emission is confined to a similar size region around the (0,0) position.

The greyscale total integrated intensity map shows considerable clumpy structure is present at this high resolution (Fig. 3a). The emission peak is close to the (0,0) position, as observed for CO and isotopes (see MWP93) but there is also an arm of emission extending along an arc southwards from the (0,0) position. There is a localised peak in emission on the PDR, at offset (-28, -42), which agrees closely with the position of the most intense localised peak on the single-channel [CI] $^3P_1 \rightarrow {}^3P_0$ map (see MWP93 Fig. 9). For the rest of the paper we shall refer to this position as PDRc1 (PDR clump 1). There is a sharp decrease in emission at the south-western edge of the map, corresponding to the molecular cloud/HII region interface.

The channel maps shown in Fig. 4 demonstrate that CI emission from the outflowing material is observed over a wide velocity range, whilst emission from the PDR is only observed at velocities -10 to -6 km s^{-1}. The channel map centred at -8 km s^{-1} compares closely with the single-channel map (using a 1.3 km s^{-1} channel centred at -8 km s^{-1}), with PDRc1 the most intense feature. The channel maps at -8 and -9 km s^{-1} confirm the conclusion of MWP93 that for the PDR in S 140 the CI emission is confined to a clumpy elongated ridge-like feature that is ~20 arcsec in width (~0.1 pc) and adjacent to the edge of the molecular cloud.

Figure 3b-d shows the integrated intensity observed in three velocity ranges, covering the blue wing (-20 to -10 km s^{-1}), core (-10 to -5 km s^{-1}) and red wing (-5 to 5 km s^{-1}) emission. Both the blue and red channel maps show a similar morphology. There is an integrated emission peak near the (0,0) position, with the redshifted peak offset to the northwest, as observed for ^{12}CO lines in similar broad velocity channels (e.g. MWP93 Figs. 6 and 7). This emission is therefore likely to be associated with the atomic component of the bipolar outflow. The arc of emission seen in total integrated intensity is prominent in both the blue and red channels, in particular the blue. The core channel shows the emission from the ambient molecular cloud and the PDR. The most striking feature is PDRc1, which is more prominent than the integrated emission peak near the (0,0) position. The contrast between the blue/red and core channels is striking. There is *no* emission from the PDR observed in the blue/red channels. There is little evidence of the emission arc in the core channel, yet it is prominent in the both the blue and red channels. It must therefore be produced by the bipolar outflow. The direction of the emission arc implies it is associated with the southern, blueshifted outflow lobe.

Figures 5 and 6 present the $C^{17}O$ J = 3→2 data. The total integrated intensity map (over the same velocity range as the CI map in shown Fig. 3a) shows a similar morphology to the CI emission. The emission arc is again prominent, as is the main emission peak near the (0,0) position. It is immediately apparent from Figs. 3a and 5a that the CI and $C^{17}O$ arc features are not coincident, with the CI arc offset to the northeast by ~10 arcsec. This will be discussed in Sect. 4.1. Broad velocity channels covering the blueshifted and core emission are shown (again over the same velocity range as the CI maps). As for the CI emission, the arc is prominent in the blue channel, but absent in core emission. The redshifted emission channel is not shown as there was a marked lack of emission from the arc feature, meaning the only feature observed in the redshifted channel is the peak near the (0,0) position. This is immediately apparent from the channel maps centred at -6.5 and -5.5 km s^{-1}. The relative lack of redshifted $C^{17}O$ emission from the arc feature will be discussed in Sect. 4.2.

3.2. The column density and abundance of CI in the outflow

The column densities of CO and CI for spectra at the (0,0) position were derived over the same velocity ranges for Figs. 3 and 5. Standard equations were used (see Phillips & Huggins

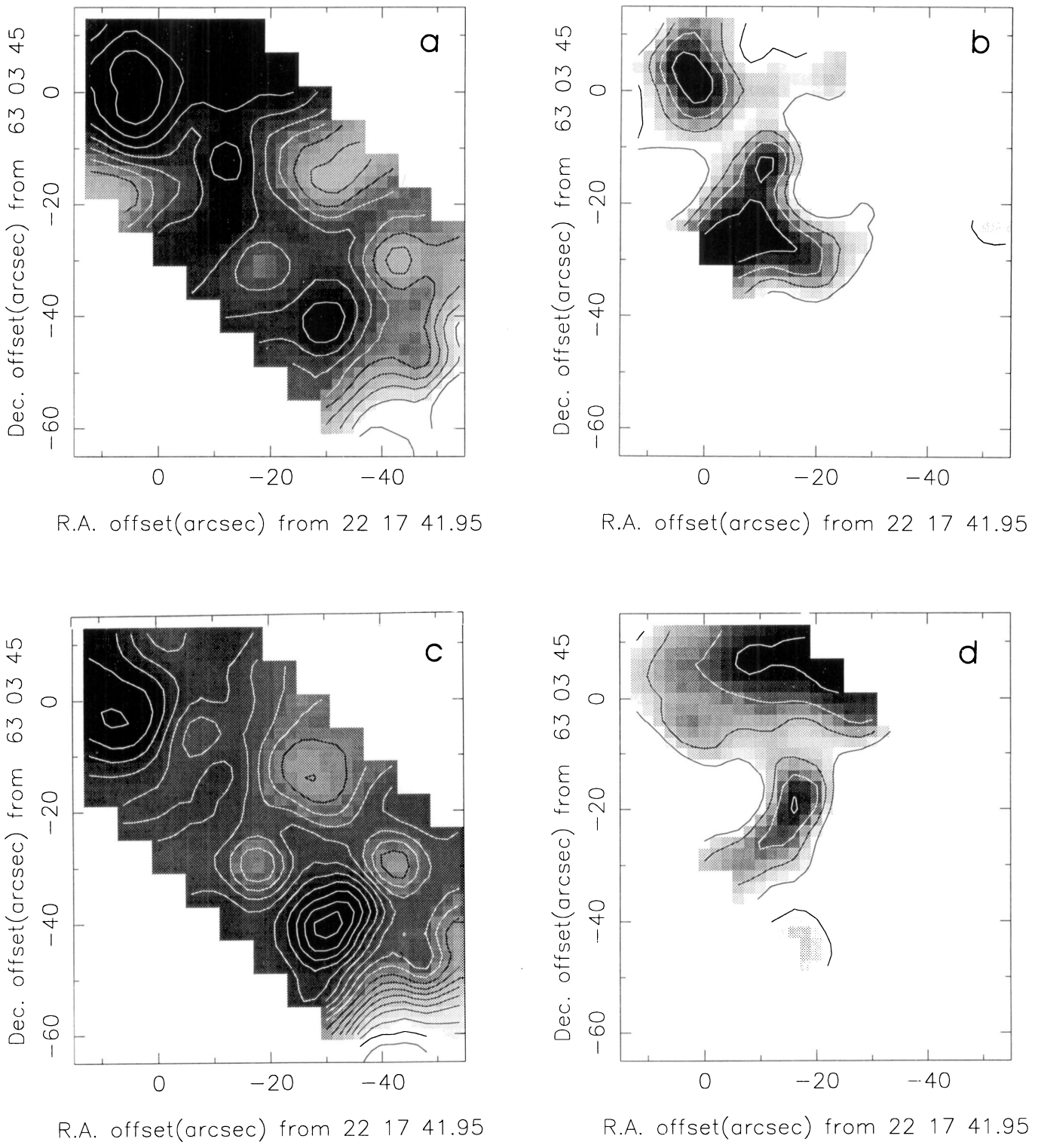

Fig. 3a–d. Greyscale images, with isophotal contours overlayed, of the [CI] $^3P_1 \rightarrow ^3P_0$ line in broad velocity channels.. Shown are the integrated intensities between **a** -14 and 2 km s^{-1}, the total integrated intensity. The base level contour is 16.8 K-km s^{-1} (3σ) and the contour interval is 5.6 K-km s^{-1} (1σ) **b** -20 and -10 km s^{-1}, the blue-shifted wing (BW). The base level contour is 9.6 K-km s^{-1} (3σ) and the contour interval is 3.2 K-km s^{-1} (1σ). **c** -10 and -5 km s^{-1}, the core emission. The base level contour is 7.1 K-km s^{-1} (3σ) and the contour interval is 2.7 K-km s^{-1} (1σ). **d** -5 and 5 km s^{-1}, the red-shifted wing (RW). The base level contour is 9.6 K-km s^{-1} (3σ) and the contour interval is 3.2 K-km s^{-1} (1σ)

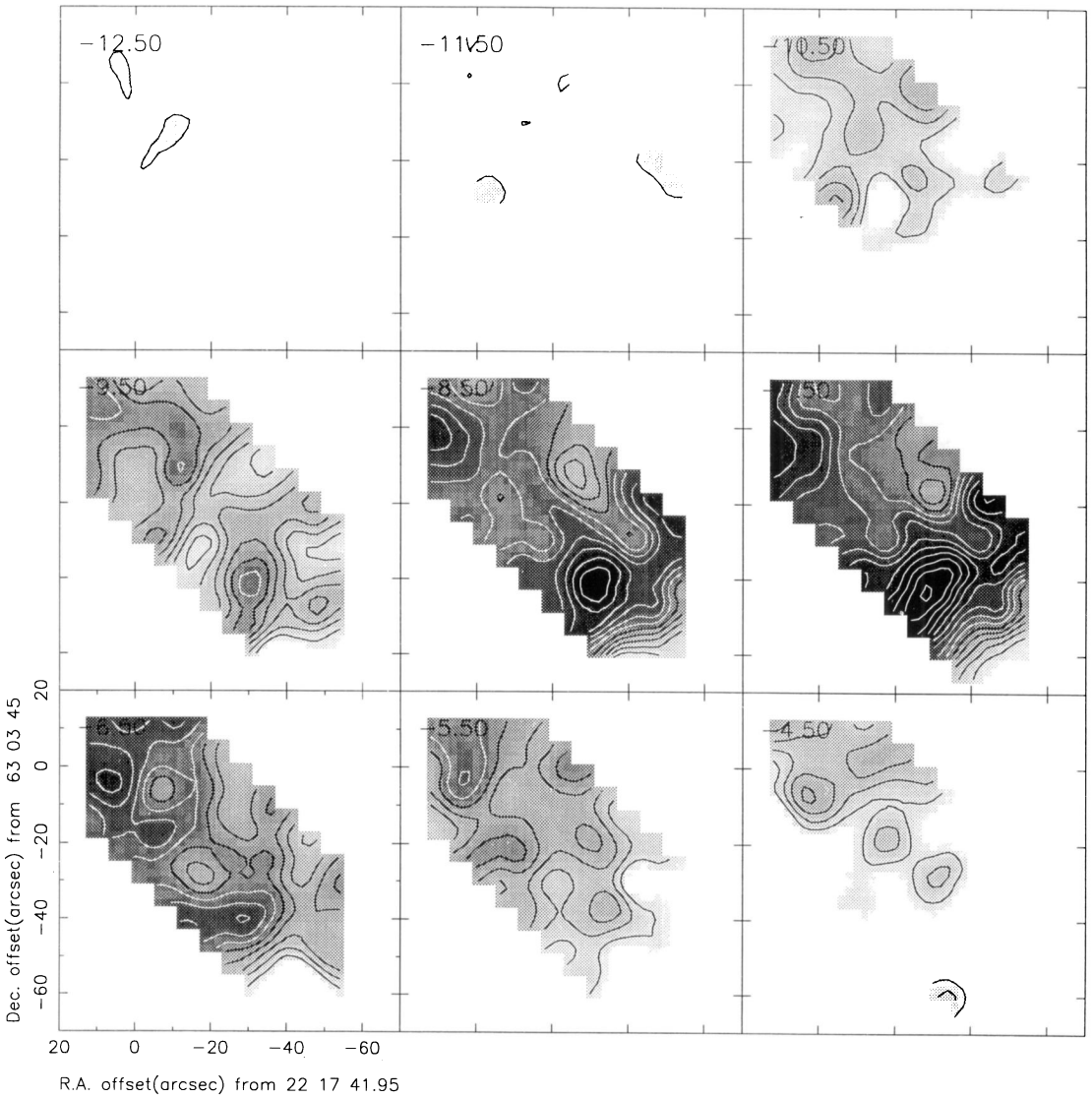

Fig. 4. Velocity channel maps for the [CI] $^3P_1 \rightarrow {}^3P_0$ line. Each map is a greyscale image, with isophotal contours overlayed. The channel width is 1 km s^{-1}, the base level contour is 3.0 K-km s^{-1} (3σ) and the contour interval is 1.0 K-km s^{-1} (1σ)

1981 and MWP93). The CO column densities were derived from the ^{13}CO J = 3→2 spectrum shown in Fig. 1a of MWP93, assuming an isotopic abundance ratio of 65 and an excitation temperature of 50K. To test for enhancement or depletion of CI relative to CO in material associated with the outflow wings *relative* to the abundance ratio found in the ambient molecular cloud, we created the ratio

$$\epsilon = \frac{N_C^{wing}/N_C^{core}}{N_{CO}^{wing}/N_{CO}^{core}} \quad (1)$$

A value of $\epsilon = 1$ will therefore indicate no net enhancement or depletion of CI relative to CO for the outflow material. The column densities, ratios and values of ϵ are given in Table 1. The abundance of CI is high, N(CI)/N(CO) = 0.14 for the full velocity range of the line and 0.12 in the blue wing and core velocity intervals. The highest value of ϵ is 5.5, observed for the red wing. For the blue wing the value of $\epsilon = 1.0$ shows that, although the abundance of CI relative to CO is high, it is not over-abundant relative to the ambient cloud material. For the red wing the value of $\epsilon = 5.6$ confirms that not only is the abundance of CI to CO high, but it is also over-abundant relative to the ambient material. These results can be compared to those of Walker et al. (1993), who found a combined value of $\epsilon = 1.1$, compared to our 1.4 for the same position in S 140. They did not derive separate ϵ values for each wing, but examination of their Table 5 implies values of $\epsilon = 0.94$ and 2.2 for the blue and red wings, respectively. Although their red wing value is lower than ours, it confirms the high over-abundance.

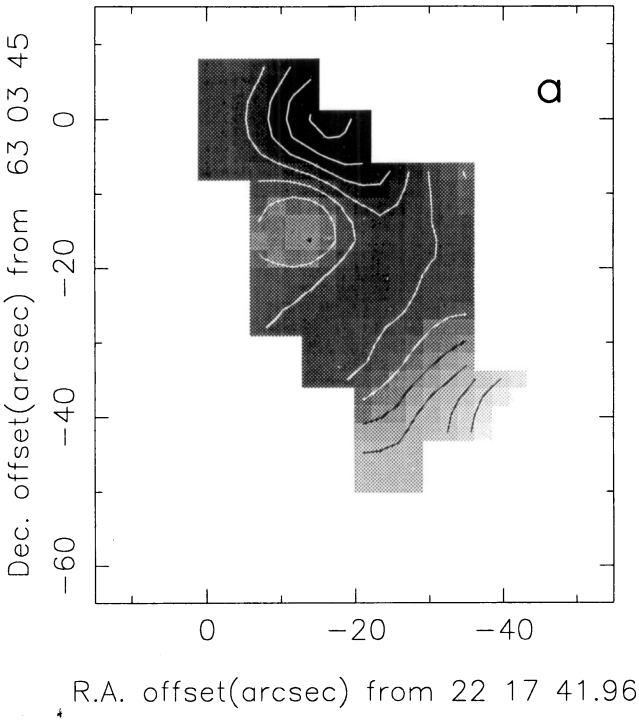

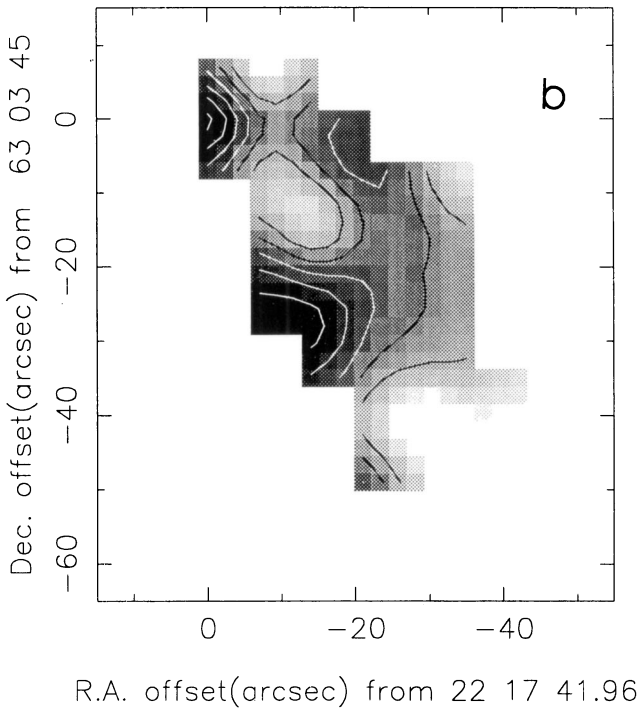

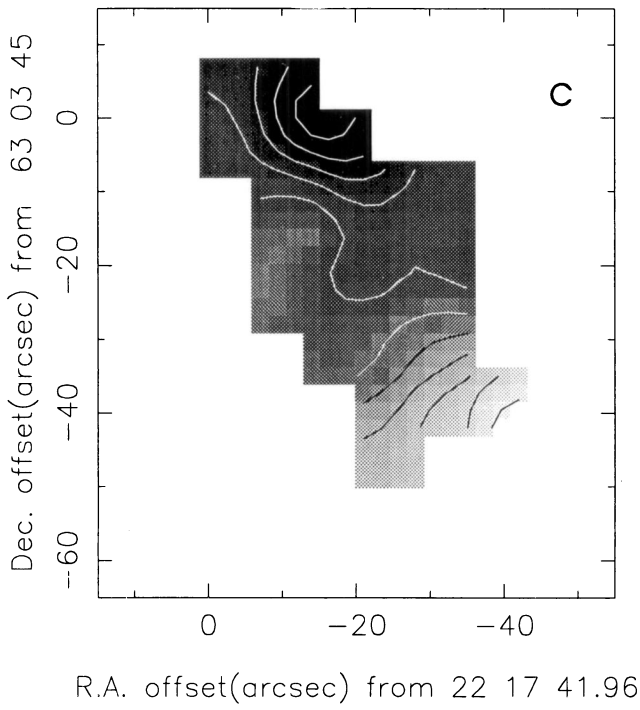

Fig. 5a–c. Observations of the J = 3→2 line of $C^{17}O$. Shown are **a** the total integrated intensity between -14 and 2 km s^{-1}. The base level contour is 3.0 K-km s^{-1} (3σ) and the contour interval is 1.0 K-km s^{-1} (1σ). **b** the total integrated intensity between -20 and -10 km s^{-1}, the blue-shifted wing (BW). The base level contour is 0.8 K-km s^{-1} (2σ) and the contour interval is 0.4 K-km s^{-1} (1σ). **c** the total integrated intensity between -20 and -10 km s^{-1}, the blue-shifted wing (BW). The base level contour is 0.8 K-km s^{-1} (3σ) and the contour interval is 0.4 K-km s^{-1} (1.5σ)

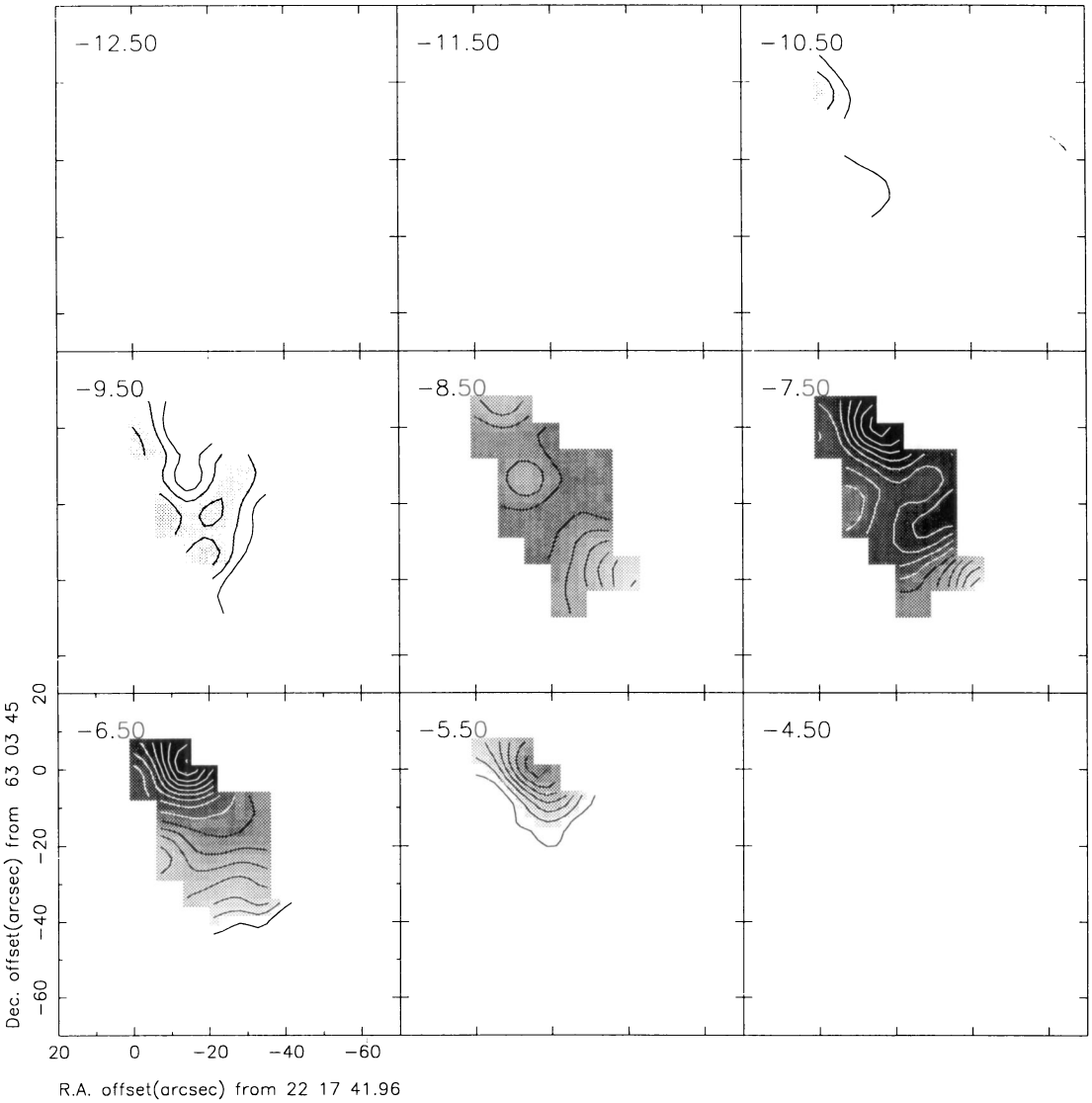

Fig. 6. Velocity channel maps for the J = 3→2 line of $C^{17}O$. Each map is a greyscale image, with isophotal conrours overlayed. The channel width is 1 km s^{-1}, the base level contour is 3.0 K-km s^{-1} (3σ) and the contour interval is 1.0 K-km s^{-1} (1σ)

Table 1. Column densities and ϵ values

	N (cm^{-2})				ϵ		
	BW	Core	RW	Total	BW	RW	Total
CI	3.7×10^{17} (±0.4)	6.6×10^{17} (±0.3)	1.9×10^{17} (±0.4)	1.2×10^{18} (±0.05)	1.0	5.6	1.4
CO	3.0×10^{18} (±0.1)	5.5×10^{18} (±0.1)	2.8×10^{17} (±1.1)	8.8×10^{18} (±0.14)			
Ratio	0.12	0.12	0.67	0.14			

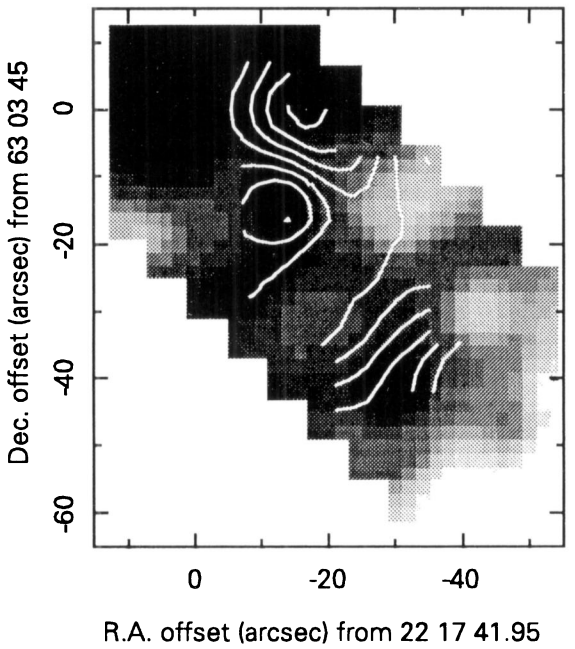

Fig. 7. Greyscale image of the total integrated intensity between -14 and 2 km s^{-1} of the [CI] $^3P_1 \rightarrow ^3P_0$ line (from Fig. 1c), with white isophotal contours of the J = 3→2 line of $C^{17}O$ overlayed (from Fig. 5a)

4. Discussion

4.1. The outflow region

As noted earlier in Sect. 3.1, the CI and $C^{17}O$ arc features appear to be offset, this can be seen clearly in Fig. 7. This shows the greyscale image of CI total integrated intensity (from Fig. 3a), with white isophotal contours of the total integrated $C^{17}O$ emission overlayed (from Fig. 5a). The CI emission arc is offset to the northeast of the corresponding $C^{17}O$ feature. The $C^{17}O$ emission appears to trace the dense, limb-brightened, blueshifted outflow cavity wall. This had not been seen in either CO or ^{13}CO emission line maps (e.g. MWP93), but is not surprising as the far higher optical depths of these lines will effectively "mask" detailed structure. The CO and ^{13}CO maps show elongated arc-like blue and redshifted emission features extending from the (0,0) position to the *north*, with a high degree of overlap (MWP93), but no southern counterpart. However, a recent high-resolution map of the HCO^+ J = 1→0 line (Wilner, private communication) shows both northern and southern arc-like features that extend from the (0,0) position, confirming the existence of the southern outflow component.

Figure 8 shows the variation in CI and $C^{17}O$ column density along two cuts. The first extends northeast-southwest from the (0,0) position to the edge of the molecular cloud, whilst the second extends along the same direction, but begins at position (0,-12). Both cuts show the twin peaks of CI column density, on the arc and the PDR, with the single $C^{17}O$ column density peak lying between. These cuts not only confirm the spatial offset of the CI and $C^{17}O$ emission arcs, but also show the limb-brightened outflow cavity wall and the PDR (as seen in CI emission) to be parallel and adjacent. Whether this is merely due to fortuitous alignment in the plane-of-the-sky, or genuine physical interaction is unclear.

Both the high abundance of CI towards the molecular outflow source (N(CI)/N(CO) = 0.28) and the over-abundance of CI found at redshifted velocities (towards the outflow source and along the emission arc) require further examination. The morphology of this region implies that the CI emission along the arc feature originates from the inner edge of the molecular outflow wall (as delineated by $C^{17}O$ and HCO^+ emission). The high abundance of CI along the inner cavity wall must therefore be due to either the dissociation of carbon-bearing molecules at the interface between the protostellar wind and the ambient medium or the accumulation of atomic carbon still present in the protostellar wind.

The effect of shocks on the chemical and physical processes at the interface between a stellar wind and the ambient cloud has been studied in a recent series of papers (McKee & Hollenbach 1987; Hollenbach & McKee 1989). Their model produces a"two-shock" structure, with an inner shock where the wind decelerates as it impacts the cavity wall and an outer shock where the ambient gas is accelerated to the shell velocity. They find that although CO has nearly three times the binding energy of H_2, CO dissociation occurs quickly afterwards as it is chemically dissociated at similar gas temperatures (≥3000K) by the endothermic reaction H + CO → C + OH. Their model predicts the intensity of the [CI] $^3P_1 \rightarrow ^3P_0$ line to be $\sim 5\text{–}7 \times 10^{-6}$ erg cm^{-2} s^{-1} sr^{-1} for pre-shock densities of 10^3–10^4 cm^{-3} and velocities 30–150 km s^{-1}. This is in good agreement with the observed values of $7\text{–}8 \times 10^{-6}$ erg cm^{-2} s^{-1} sr^{-1} along the arc of CI emission (within the error of $\sim 1\text{-}1.5 \times 10^{-6}$ erg cm^{-2} s^{-1} sr^{-1}).

Towards the outflow source itself (the 0,0 position) the intensity of CI emission is even higher $\sim 1 \pm 0.05 \times 10^{-5}$ erg cm^{-2} s^{-1} sr^{-1}. The enhancement here may be due to a high concentration of atomic carbon in the atomic wind close to the outflow source, as the wind expands into the outflow cavity it cools, leading to the formation of molecules (predominantly CO). Recent modelling by Glassgold et al. (1991) imply that for large mass-loss rates (10^{-5}–10^{-6} $M_\odot$ yr^{-1}) the wind is essentially molecular, but for lower rates ($\leq 10^{-6}$ $M_\odot$ yr^{-1}) the abundance of CI is significant and often greater than that of CO. Snell et al. (1984) use their CO J = 2→1 and 1→0 observations to calculate the mass-loss rate in the S 140 outflow to be 1×10^{-4} $M_\odot$ yr^{-1}, assuming a stellar wind velocity of 100 km s^{-1}. They also point out that this is distinctly lower than the rate calculated from the radio continuum (between 4×10^{-7} and 1×10^{-6} $M_\odot$ yr^{-1}). The most plausible explanation put forward by Snell et al. for the discrepancy is a significant mass of neutral material in the wind, consistent with our observation of enhanced CI intensity at the (0,0) position. It should also be noted that close to the young star the UV radiation field will be sufficiently intense to photodissociate CO, enhancing the observed CI abundance. If the abundance of CI in the outflow wind is significant and survives until the interaction of the wind with the cavity wall, this

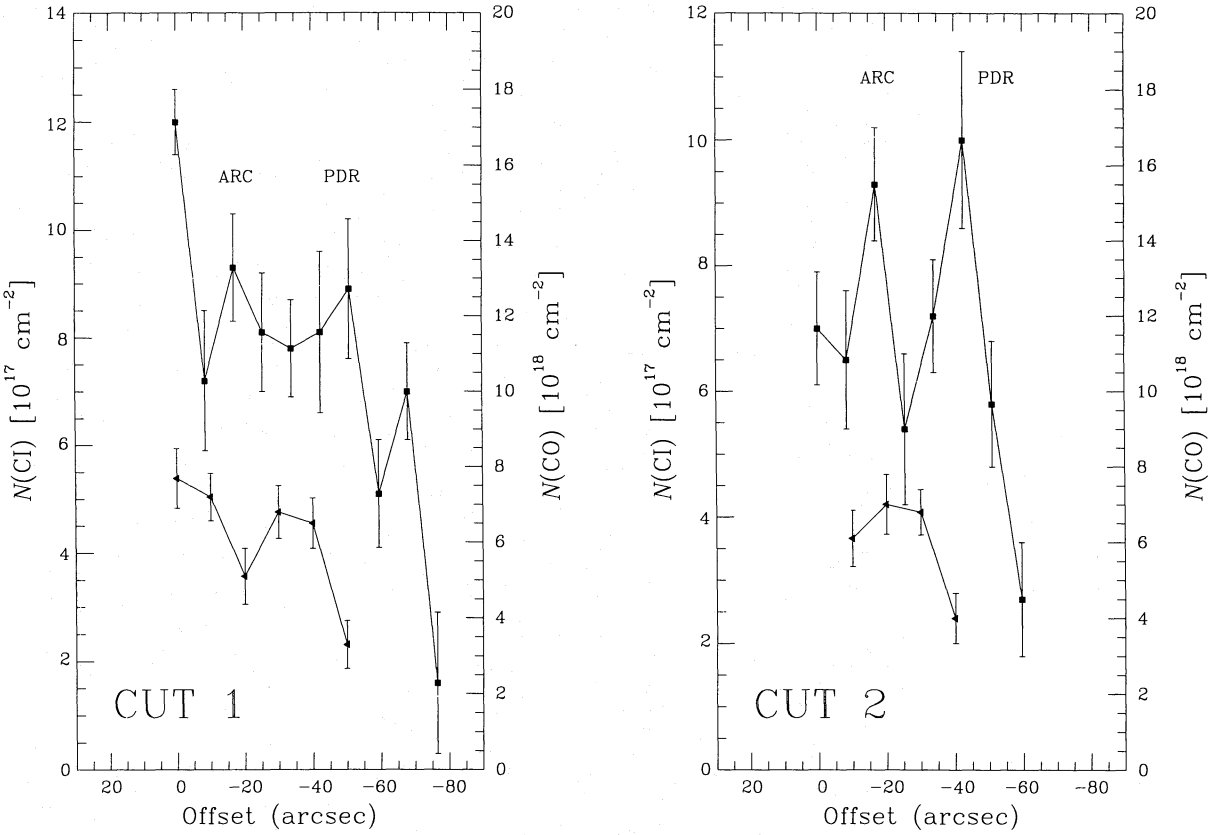

Fig. 8. The variation of [CI] $^3P_1 \rightarrow {}^3P_0$ and $C^{17}O$ J = 3→2 column density along two cuts. Cut 1 extends northeast-southwest from the (0,0) position to edge of the molecular cloud. Cut 2 is along the same direction, but begins at offset position (0,-12). The CI and CO data points are plotted as solid squares and triangles respectively. The position of the CI emission arc and the PDR are labelled

may account for the arc feature. The main problems with this scenario is that it does not explain the apparent offset of the CI and $C^{17}O$ emission arms and also the presence of redshifted CI emission, but no CO counterpart.

The fact that the CI arc feature is seen in both blue and redshifted emission cannot be a geometrical effect. The observation of both blue and redshifted emission along certain lines of sight towards molecular outflows has been previously noted. This is usually attributed to either a particularly wide opening angle for the outflow lobes or the outflow axis being directed close to the observers line-of-sight. This cannot be the case here as we do not observe redshifted $C^{17}O$ emission from the arc feature. If both the CO and CI emission trace the outflow cavity wall then they should both demonstrate similar velocity structure. The obvious implication is that both the observed blue and redshifted CI emission is produced at the same position, along the inner edge of the cavity wall for the *blueshifted* lobe of the molecular outflow. This scenario may also explain the over-abundance of CI relative to CO at redshifted velocities. As Hollenbach & McKee (1989) point out, one of the signatures of shocks is the presence of broad emission lines arising from the large dispersion in velocity vectors, in contrast with PDRs which have narrow lines, of the order of the turbulent velocity of the ambient gas. Where the wind interacts with the cavity wall the resultant ionized and dissociated material will be accelerated over a range of velocities about the original velocity of the ambient material. This will be observed as both blue and redshifted wings on emission lines emitted as the material cools. Hence both blue and redshifted CI emission may be present at positions on the outflow where *only* blue *or* redshifted CO emission is observed.

Although the observed CI lines are much narrower (FWHM ~5–6 km s^{-1}, with blue and red wings that extend over ~20 km s^{-1}) than lines of H_2 or OI from shock excited regions (FWHM ~50 km s^{-1}), they are closely comparable with recent [CI] $^3P_1 \rightarrow {}^3P_0$ line observations of the DR21 and BN/KL outflows (Walker et al. 1993; White 1994a). Both of these regions have well-known examples of outflows that exhibit numerous shock-excited emission lines. To our knowledge the present observations represent the broadest [CI] $^3P_1 \rightarrow {}^3P_0$ lines to be observed from a molecular outflow. Broader CI lines have been observed recently towards IC443 (FWHM ~60 km s^{-1}; White 1994b). Of course ^{12}CO and ^{13}CO lines observed from IC443 are also similarly broad, yet the ^{12}CO and ^{13}CO lines observed towards S 140 are much narrower, comparable to our observed CI lines. Faint high-velocity wings may be present in CI emission from outflows, but the present observations (and those of Walker et al. 1993 and White 1994a) did not obtain sufficient S/N to test this possibility.

4.2. CI emission from the PDR

The new [CI] $^3P_1 \rightarrow ^3P_0$ line observations confirm the earlier single-channel observations (White & Padman 1991; MWP93). The PDR is an elongated, narrow (~0.1-0.15pc) ridge-like feature that is adjacent to the south-western edge of the molecular cloud. CI emission from the PDR is only observed for velocities -10 to -6 km s^{-1}, and mainly at velocities -9 to -7 km s^{-1} (Fig. 4). Unfortunately our mapped area is smaller than the single channel map, but it is still obvious that the PDR is extremely clumpy, with PDRc1 the dominant emission feature. There is a sharp decrease in emission at the south-western edge of the PDR, corresponding to the molecular cloud/HII region interface.

The close agreement between the new CI map and the original single-channel observations mean that many of the conclusions by MWP93 are confirmed. The CI and ^{12}CO emission "ridges" are coincident (see Fig. 14 of MWP93). This contradicts the original homogeneous cloud models for PDRs (e.g. Tielens & Hollenbach 1985; van Dishoeck & Black 1988) where CI and ^{12}CO are predicted to be in distinct, adjacent layers, with the CO deeper into the molecular cloud. The coincidence of the CI and ^{12}CO ridges and the observed clumpy structure of the CI ridge imply that a multi-component model is appropriate. Such models predict that molecular cloud material is composed of distinct high density clumps, interspersed with a more tenuous interclump medium. UV radiation can penetrate deep into the cloud before heating and dissociating carbon-bearing molecules on molecular clump surfaces.

For PDRc1 we derived a CI column density of $9.7\pm0.8\times10^{17}$ cm^{-2} and N(CI)/N(CO) = 0.29. These were derived using the C^{17}O spectra obtained at the same position and assuming isotopic abundance ratios of ^{12}CO/C^{18}O = 500 and C^{18}O/C^{17}O = 3.5. The emergent intensity at the position of PDRc1 is $8.7\pm0.7\times10^{-6}$ erg cm^{-2} s^{-1} sr^{-1}. These values are in close agreement with the conclusions of Hollenbach et al. (1991) that [CI] $^3P_1 \rightarrow ^3P_0$ line emission from low-density PDRs ($10^2 \leq n_0 \leq 10^5$ cm^{-3}), such as S 140, should have an emergent intensity of ~10^{-5} erg cm^{-2} s^{-1} sr^{-1} and a column density of ~10^{18} cm^{-2}, relatively independent of the incident FUV flux and the density of the cloud.

5. Conclusions

We have mapped the S 140 bipolar outflow and PDR in the [CI] $^3P_1 \rightarrow ^3P_0$ and C^{17}O J = 3→2 emission lines.

There is a marked variation in CI line profiles across the mapped region. Towards the outflow the lines are broad (FWHM ~5-6 km s^{-1}) with peak values of T_{mb} ~10-12K, yet towards the PDR the lines are distinctly narrower (~3-4 km s^{-1}) with higher values of peak T_{mb}, up to 18K.

CI is highly-abundant towards the molecular outflow source, N(CI)/N(CO) = 0.14. A similar abundance is found for the blue wing and core velocity intervals (0.12), but for the red wing the abundance is remarkably high, N(CI)/N(CO) = 0.67. There is no net enhancement of the blue wing material relative to the ambient cloud material (signified by $\epsilon = 1.0$) which shows that, although the abundance of CI relative to CO is high, it is not over-abundant relative to the ambient cloud material. For the red wing the value of $\epsilon = 5.6$ confirms that not only is the abundance of CI to CO extremely high, but it is highly over-abundant relative to the ambient material.

Both the CI and C^{17}O integrated intensity maps show a similar morphology. The emission peak lies towards the molecular outflow source, and there is an arc of emission extending from the peak towards the south. The CI and C^{17}O arcs are offset, with the CI arc offset to the northeast by ~10 arcsec. The CI arc feature is observed in blue and redshifted emission, whilst the C^{17}O arc feature is only observed in blueshifted emission. This implies the CI emission arc traces the inner edge of the blueshifted molecular outflow wall (traced by the C^{17}O emission).

The most plausible mechanism for producing the CI emission is the effect of shocks on the chemical and physical processes at the interface between the stellar wind and the blueshifted outflow cavity wall.

The PDR is a clumpy, narrow (~0.1–0.15pc) elongated ridge-like feature, adjacent to the south-western edge of the molecular cloud. Emission from the PDR is observed within a relatively narrow velocity range, -10 to -6 km s^{-1}. There is a localised peak in emission at offset position (-28,-42), which we have designated PDRc1 (PDR clump 1). PDRc1 is a more prominent emission feature than the outflow peak over the velocity range -9 to -7 km s^{-1}. The abundance of CI is high, N(CI)/N(CO) = 0.29 at the position of PDRc1. The observed column density ($9.7\pm0.8\times10^{17}$ cm^{-2}) and emergent intensity ($8.7\pm0.7\times10^{-6}$ erg cm^{-2} s^{-1} sr^{-1}) towards PDRc1 are in close agreement with recent modelling of low-density PDRs.

Acknowledgements. We wish to thank Adrian Russell and Andrew Harris for their help in taking some of the CI spectra. We acknowledge the SERC for travel funds, and NRM's PDRA.

References

Bally J., Lada C., 1983, ApJ 265, 824
Beichman C. A., Becklin E. E., Wynn-Williams C. G., 1979, ApJ Lett 232, L47
Blair G. N., Evans N. J., Vanden Bout P. A, Peters W. L., 1978, ApJ 219, 896
van Dishoeck E. F., Black J. H., 1988
Evans N. J., Kutner M. L., Mundy L. G., 1987, ApJ 323, 145
Glassgold A. E., Mamon G. A., Huggins P. J., 1991, ApJ 373, 254
Hernichel J., Krause D., Rohrig R., Stutzki J., Winnewisser G., 1992, A&A 259, L77
Hollenbach D. J., McKee C. F., 1989, ApJ 342, 306
Hollenbach D. J., Takahashi T., Tielens A. G. G. M., 1991, ApJ 377, 192
Keene J., Blake A., Phillips T. G., Huggins P. J., Beichman C. A., 1985, ApJ 299, 967
Langer W., 1976, ApJ 206, 699
McKee C. F., Hollenbach D. J., 1987, ApJ 322, 275
Minchin N. R., White G. J., Padman R., 1993, A&A 277, 595 (MWP93)
Phillips T. G., Huggins P. J., 1981, ApJ 251, 533

Prasad S. S., Huntress W. T., 1980, ApJS 43, 1
Snell R. L., Scoville N. Z., Sanders D. B., Erickson N. R., 1984, ApJ 284, 176
Stutzki J., Stacey G. J., Genzel R., Harris A. I., Jaffe D. T., Lugten J. B., 1988, ApJ 332, 379
Tielens A. G. G. M., Hollenbach D. J., 1985, ApJ 291, 722
Walker C. K., Narayanan G., Buttgenbach T. H., Carlstrom J. E., Keene J., Phillips T. G., 1993, ApJ 415, 672
White G. J., 1988, In: Millimetre and Submillimetre Astronomy, eds. Wolstencroft R. D., Burton W. B., Kluwer, p. 27
White G. J., Padman R., 1991, Nat 354, 511
White G. J., 1994a, A&A submitted
White G. J., 1994b, A&A in press
Wootten A., Phillips T. G., Beichman C. A., Frerking M., 1982, ApJ 256, L5

This article was processed by the author using Springer-Verlag LaTeX A&A style file version 3.